

Location dependent flight costs from the lunar surface to an orbital fuel depot and its influence on ISRU location selection

Sven J. Steinert^{1,*}, Paul Zabel² and Dominik Quantius²

¹*School of Engineering and Design, Technical University of Munich (TUM), Munich, Germany*

²*Institute of Space Systems, Systemanalyse Raumsegment, German Aerospace Center (DLR), Bremen, Germany*

Correspondence*:

Sven Julius Steinert

sven.julius.steinert@outlook.com

2 ABSTRACT

To raise information about the dominant location dependencies, a scenario was set up where an ISRU product is exported to an orbital depot and mass costs are used for classification. In the selected scenario, Oxygen is produced by an Ilmenite reduction plant and subsequently exported to the Lunar Gateway via an Oxygen-Hydrogen fueled launcher running in a round-trip, refueling Oxygen at the lunar surface and Hydrogen at the Lunar Gateway. It showed that the variations in transport costs can be either entirely avoided or have a recessive influence on the missions total costs over an extented amount of time as 20 years. The identification of the top 10 most optimal locations were only altered slightly under consideration of flight costs, even both considerations delivering the identical location as the number 1 ranked outcome.

Keywords: **In situ resource utilization (ISRU), in-orbit fuel depot, lunar outpost, location selection, delta v map, Ilmenite reduction, Lunar Gateway, NRHO**

1 INTRODUCTION

When a fully robotic In situ resource utilization (ISRU) plant is feasible on the lunar surface, the location selection is not anymore bound to life support systems and the water resources they require. Therefore an optimization on the process factors can be applied to pick the most optimal location globally, instead being limited to polar regions only. For this event, this analysis is trying to identify the leading significance of the two sections of process factors, the ISRU efficiency (Section 3) and the Transport efficiency (Section 4) under the aspect of exporting the ISRU products. Hereby each section is inspected separately first before they are combined in a joined model (Section 5) to conclude the more relevant influence in Section 6.

2 MATERIALS AND METHODS

21 **2.1 Methods**

22 **2.2 Scenario**

23 In particular the ISRU production plant produces Oxygen as propellant component that is exported to
24 an orbital propellant depot. The annual Oxygen production is 23.9 t (Chapter 3.1) that is transported via
25 a round trip of a rocket launch system (Chapter 4.5) over [x] runs annually to the fuel-depot at target
26 destination (Chapter 4.2). The mission duration is designed over a period of 10 years.

27 **2.3 Material**

3 ISRU EFFICIENCY

When the optimal location is chosen by the highest ISRU efficiency, the whole production line has to be inspected for location dependent factors first. Such location dependent factors are for example: raw material concentration, solar irradiance, temperatures, flat surface conditions and further scenic requirements. Hereby, the production method is decisive about the sensitivity to location dependend factors. Where hydrogen reduction of ilmenite features a high dependency on the raw material concentration, molten regolith electrolysis for example is mostly invariant to it over the lunar surface. In this paper hydrogen reduction of ilmenite is chosen as the production method to be analysed, which we expect to have a rather strong location dependency. All results that are derived here are therefore only applicable to this single production method.

3.1 Model

To simplify model complexity, our model does include only the raw material concentration factor as argument, the Ilmenite weight ratio. While not covering all influences, this factor we are assuming the most significant for location dependency and serves as our approximation to the full model of hydrogen reduction of ilmenite. The goal here is not to give a precise value but to get in the right order of magnitude for a comparison later. The model cost is defined as the hardware mass that has to be moved to the lunar surface for ISRU operation which is to be minimized. In a previous work of (Guerrero-Gonzalez and Zabel, 2023) this hardware mass depending on Ilmenite concentration was determined for a combined production plant of Low Carbon Steel and Oxygen production. This production plant was sized for an annually output of 23.9 t Oxygen and 25 t Low Carbon Steel. The model consists out of a sum of required subsystems as defined in Equation 1 below.

$$\begin{aligned}
 y_0(x) &= 4036 \cdot x^{-1.064} - 9.59 && \text{Excavation} \\
 y_1(x) &= 17580 \cdot x^{-1.003} - 390.8 && \text{Handling} \\
 y_2(x) &= 19240 \cdot x^{-1.003} - 421.9 && \text{Beneficiation} \\
 y_3(x) &= 21780 \cdot x^{-1.198} + 120.3 && \text{O2 Extraction} \\
 y_4(x) &= 17910 \cdot x^{-1.265} + 1370 && \text{O2 Purification} \\
 y_5(x) &= 29650 \cdot x^{-0.7005} - 602.5 && \text{Metal Processing} \\
 y_6(x) &= 2541 \cdot x^{-0.7434} + 286.8 && \text{Gas Liquefaction \& Storage} \\
 y_7(x) &= 32440 \cdot x^{-0.8312} + 125.2 && \text{Thermal Control} \\
 y_8(x) &= 12000 \cdot x^{-0.9657} + 63.99 && \text{Power}
 \end{aligned}$$

48

$$m_{\text{hardware}}(x = w_{\text{ilmenite}}) = \sum_{i=0}^8 y_i(x) \quad (1)$$

Where in our scenario only the Oxygen production is relevant, the additional subsystems as Metal Processing scale in a similar way as the rest of the system so that the spread between low and high values of x is not distorted significantly (88.69% spread to the maximum value vs. 89.97% spread without Metal Processing, with $1 \leq x \leq 11$). Furthermore this combined production plant could still be a viable choice

53 out of the synergetic effects of shared infrastructure. This is why we are choosing this to be our reference
 54 production plant as a whole rather than attempting trimming subsystems. Therefore our model is expressed
 55 in Equation 1 as well.

56 3.2 Data Processing

57 To determine the cost for every location on the moon, a global lunar map of Ilmenite weight ratio is
 58 required. In a previous work by Hiroyuki (Sato et al., 2017) an almost global TiO₂ abundance map was
 59 created, where the values of weight percent for TiO₂ are used as equivalent for Ilmenite. The resulting
 60 map had a mask applied to leave only lunar mare regions and had a limited latitude coverage from 70° S to
 61 70° N. The limited coverage is caused by the sensor method to measure the reflectance of sunlight which
 62 is working less reliable with an increasingly steep sunlight angle towards the poles. The initial data was
 63 created by the Lunar Reconnaissance Orbiter Camera (LROC) Wide Angle Camera (WAC) which will be
 64 our starting point for the creation of our global Ilmenite map. First, the WAC data segments have been
 65 joined together resulting in a 27360 × 10640 resolution of 8-bit encoded values, plotted in Figure 1 below.

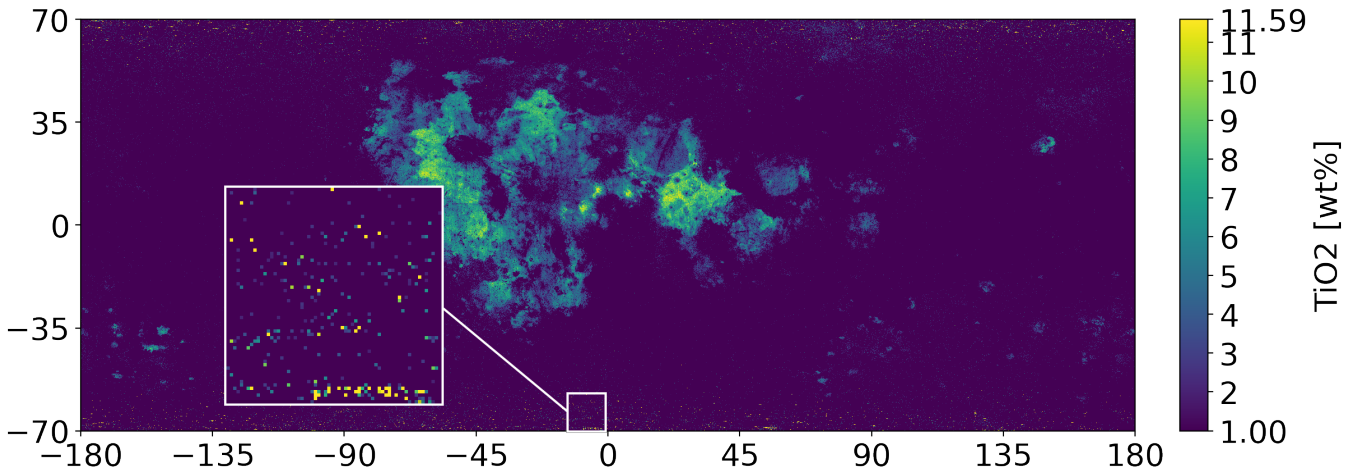


Figure 1. Combined original TiO₂ data of the WAC, (Sato et al., 2017)

66 3.2.1 Cleanup and Estimation

67 One problem are unusual high measurements towards the poles that are considered increasing noise
 68 which is scattered through the entire longitudinal axis. The second problem is the incomplete coverage of
 69 latitude and therefore the poles itself. To derive an estimation over the missing information at latitudinal
 70 coverage, the following strategy was applied. If Ilmenite abundance correlates with the classification of
 71 highlands/ mare and the pole regions geology is featuring highland characteristics then the expected value
 72 of the known highland region serves as an estimate of Ilmenite content at the poles.

73 As Figure 2 shows, the distribution characteristics of these two regions deviate considerably, whereby
 74 the average abundance also differs from 3,38 wt% in Mare to 1,1 wt% in Highland regions. Therefore the
 75 Ilmenite content correlation is given and the estimate over the missing latitudinal area of Highlands is set to
 76 1 wt% which also matches the WAC original assumption for values under the detection ratio. To additionally
 77 remove the increasing noise at further extreme latitudes, a mask is created out of mare boundaries from
 78 (Nelson et al., 2014) merged with a constant separation at ±56 deg latitude. The replacement values

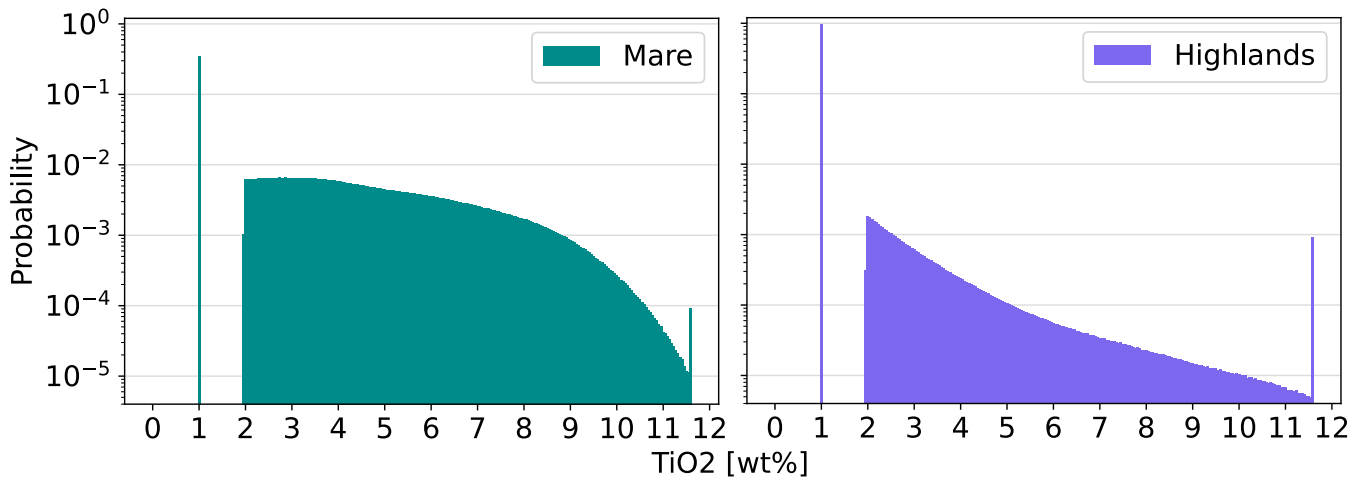


Figure 2. Distribution of Ilmenite content clustered into Highlands and Mare (equirectangular corrected) on combined WAC data with Mare boundaries from (Nelson et al., 2014)

79 for the mask are equally set to 1 wt%. With both estimates applied, a low noise global Ilmenite map is
80 accomplished which can be seen in Figure 3 below.

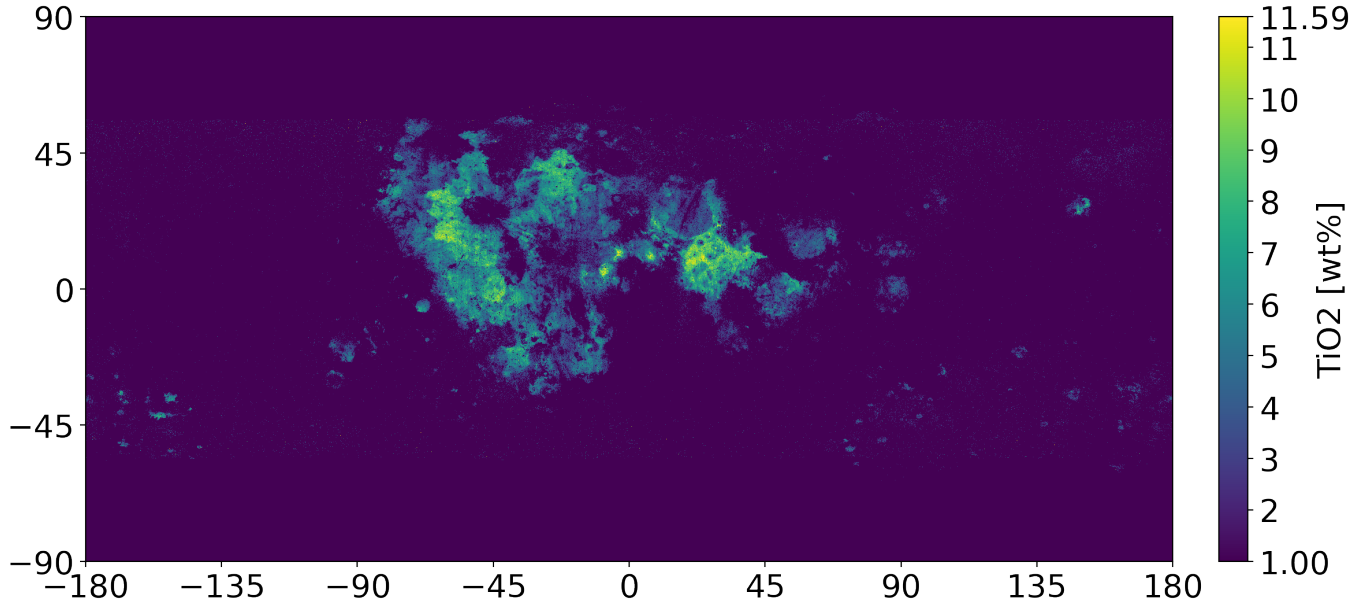


Figure 3. Location dependent Ilmenite weight percent through TiO₂, based on WAC data and estimates

81 3.2.2 Result

82 This global Ilmenite map from Figure 3 is now used as input to Equation 1, which results in the global
83 ISRU cost map displayed in Figure 4.

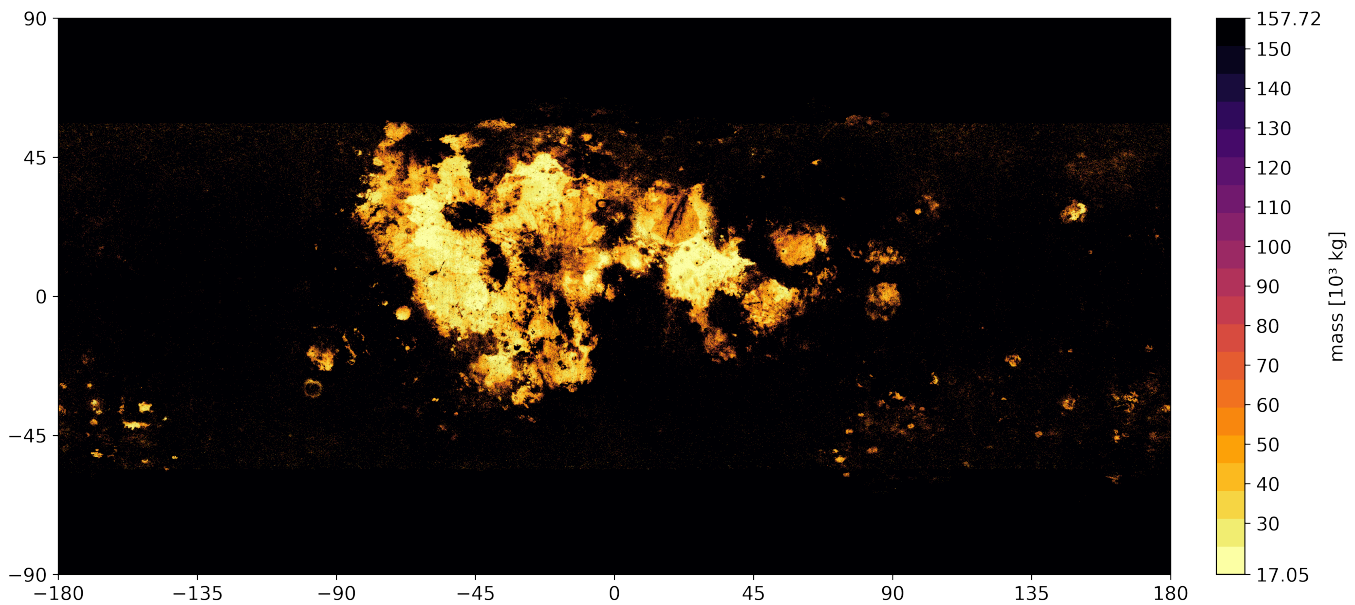


Figure 4. Location dependent ISRU hardware mass costs K_{base} in its base configuration of 23.9 t Oxygen per year

4 TRANSPORT EFFICIENCY

85 4.1 Mission Planning

86 The mission is designed to be carried out by a single stage launcher to loop between the lunar surface
 87 and the target orbit destination. The Oxygen fuel component and the Oxygen payload are refilled on lunar
 88 ground at the ISRU production plant. The Hydrogen fuel component on the other hand is refilled at the
 89 fuel depot where also the Oxygen payload is delivered. This results effectively in an exchange of delivered
 90 Oxygen to deducted Hydrogen from the station. A multi staged launcher or a shuttle exchange system was
 91 neglected for this analysis but would hold the potential to further increase transport efficiency.

92 4.2 In Orbit Fuel Depot Location

93 The primary requirement of the fuel depot location is its accessibility from both the supplying and
 94 consuming units. For an interplanetary logistic hub near earth, Liberation points are especially suited as
 95 considered by previous studies Perrin and Casler (2016). Similar to Liberation points, their corresponding
 96 Halo orbits are offering the benefits of accessibility as well. In the case for an interplanetary logistic
 97 hub near earth which is supplied by the lunar surface, the currently planned Lunar Gateway on its Near-
 98 rectilinear halo orbit (NRHO) fits prodigiously as a theoretical test bed for this purpose. Which is why the
 99 Lunar Gateway orbit is chosen to be analysed in this scenario as the export destination and considered a
 100 fuel depot.

101 4.3 Target Orbit

102 For the selected fuel depot location at the Lunar Gateway, the target orbit is a specific NRHO that is in a
 103 9:2 Lunar Synodic Resonance with an average perilune of $h_{peri} = 3557 \text{ km}$ and an average orbital period
 104 of $T = 6.562 \text{ days}$ (Lee, 2019). It is worth mentioning that this orbit has a varying polar crossing as well
 105 as other time dependent changes in its trajectory which are often simplified to more static conditions for
 106 analysis (Whitley et al., 2018).

107 4.4 Δv Estimation

108 First of all, regardless of the mission or the trajectory, planetary conditions such as ground elevation and
 109 ground speed are influencing the required Δv . These influences are now briefly assessed for the moon to
 110 determine their relevance.

111 4.4.1 Planetary influences

112 The initial radial distance to the planets center of mass $r(\phi, \lambda)$ influences the Δv demand directly as
 113 shown for an ascent into a circular orbit at r_{orbit} in equation 2 below.

$$\Delta v_{ideal}(\phi, \lambda) = \sqrt{v_{orbit}^2 + v_{ascent}^2} = \sqrt{\left(\frac{\mu}{r_{orbit}}\right) + \left(2 \cdot g_0 \cdot \left[r(\phi, \lambda) - \frac{r(\phi, \lambda)^2}{r_{orbit}}\right]\right)} \quad (2)$$

114 Global ground elevation data is now used in the form of a displacement map, which originates on LOLA
 115 measurements. The elevation ranges from -9.115 km to 10.757 km with regard to the reference radius r_{ref}
 116 of 1737.4 km and therefore defines $r(\phi, \lambda)$ globally. The displacement map is shown in Figure 5 below.

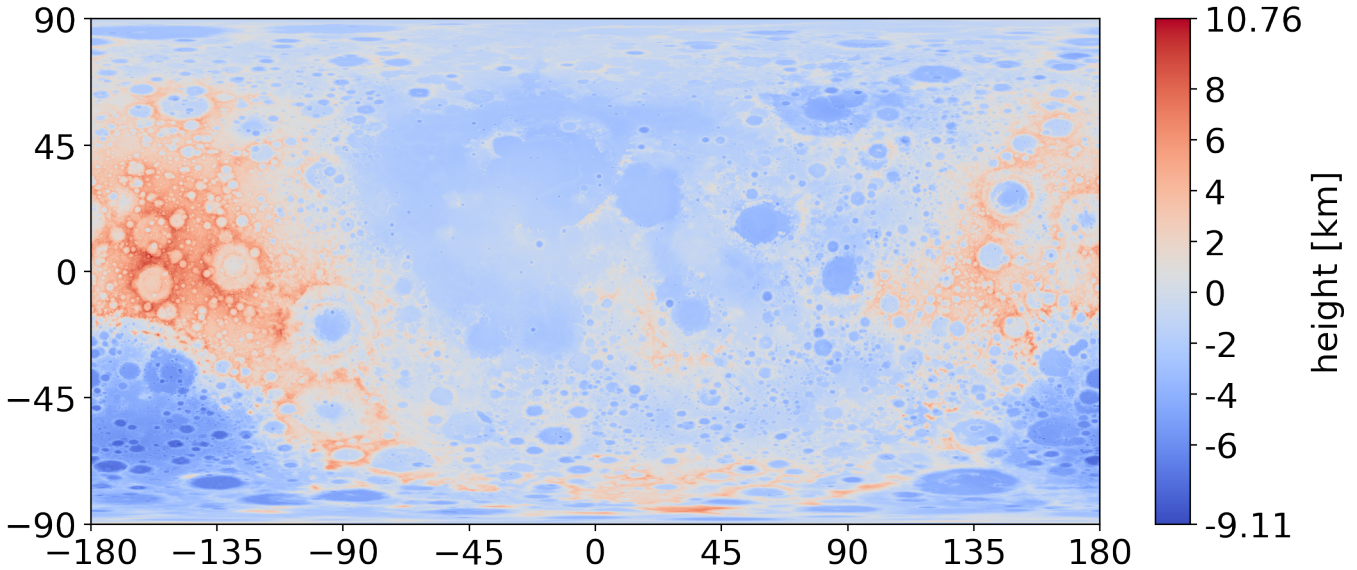


Figure 5. Lunar displacement map to reference radius ($r_{\text{ref}} = 1737.4 \text{ km}$). Data from NASA CGI Kit (Ernie Wright and Noah Petro, 2019) based on (David E. Smith, 2015)

Evaluating the extreme values with Equation 2 on a 100 km LLO ($r_{\text{orbit}} = 1837.4 \text{ km}$) yields:

$$\Delta v_{\min} = \Delta v_{\text{ideal}}(\max \{r(\phi, \lambda)\}) = 1725.187 \frac{\text{m}}{\text{s}}$$

$$\Delta v_{\max} = \Delta v_{\text{ideal}}(\min \{r(\phi, \lambda)\}) = 1725.204 \frac{\text{m}}{\text{s}}$$

117 The influence on Δv from ground elevation is therefore at the order of 0.001 % which is extremely low.
 118 The second planetary influence, the initial ground speed v_0 is either an additional Δv demand or a Δv
 119 reduction, depending on the shared velocity components to the launch direction. Together with the sidereal
 120 rotation period and the assumption of a spherical lunar surface of r_{ref} , the ground speed can be given as a
 121 function of Latitude ϕ as displayed in Equation 3.

$$v_0(\phi) = \frac{2\pi}{27.322 \text{ days}} \cdot \cos(\phi) \cdot r_{\text{ref}} \quad (3)$$

122 Evaluating the extreme points of polar and equatorial locations on Equation 3 yields:

$$\Delta v_{\min} = \Delta v_0(\phi = 90 \text{ deg}) = 0.000 \frac{\text{m}}{\text{s}}$$

$$\Delta v_{\max} = \Delta v_0(\phi = 0 \text{ deg}) = 4.624 \frac{\text{m}}{\text{s}}$$

123 Comparing this range $\Delta v_{\max} - \Delta v_{\min}$ to the ascent of a circular 100 km LLO to reference radius
 124 $\Delta v_{\text{ideal}}(r_{\text{ref}}) = 1725.196 \frac{\text{m}}{\text{s}}$ gives the Δv influence of the ground speed to be at the order of 0.27 % which
 125 is significantly more than the elevation influences but still considerably low.

126 4.4.2 Transfer options

127 Explicit Transfers from any lunar geodetic point to NRHOs and vice versa are a high-fidelity problem
 128 which is usually solved non-analytically. Additionally there are multiple transfer strategies that can be

129 deployed for different optimisation goals. Between optimisation of required Δv and transfer time, 2 transfer
 130 options are being analysed for our chosen scenario.

131 First, a long duration transfer that features a very low required Δv of only $664.9 \frac{m}{s}$ to a 100 km LLO,
 132 which is very close to the theoretical limit of $654.8 \frac{m}{s}$ as minimum energy change (Whitley et al., 2018).
 133 Also, it features an almost complete independency to surface location, which is reached by something
 134 similar as a Three-Impulse transfer, where the lunar sphere of influence is left to circle once around earth
 135 before inserting again. This allows any inclination restrictions to vanish, but at a cost of a 100.1 day long
 136 transfer time. This first, long transfer option is displayed in Figure 6 below.

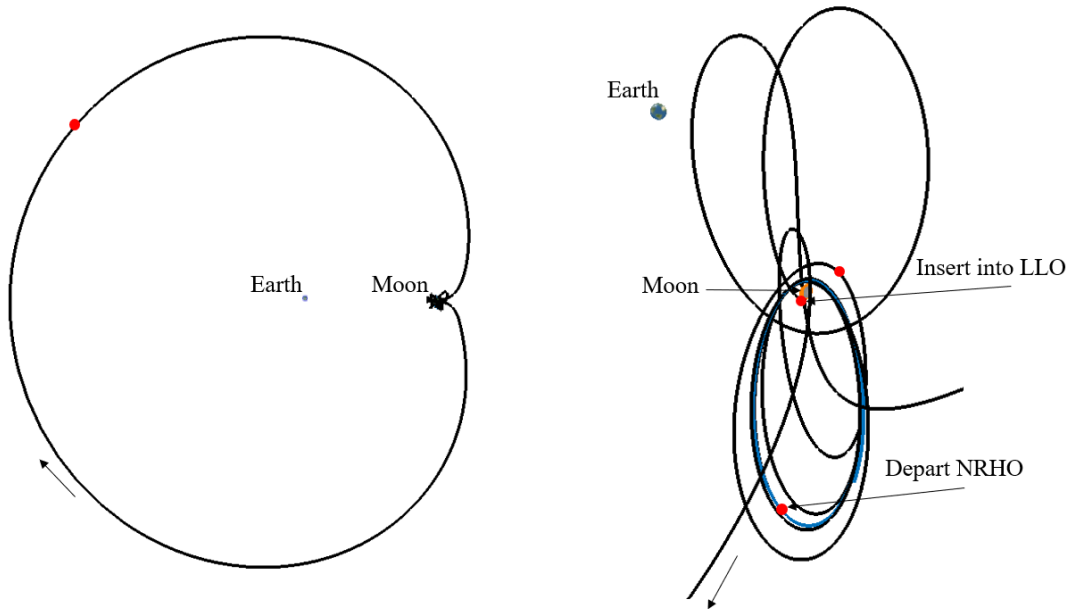


Figure 6. “100.1 day transfer from the 9:2 NRHO to 100 km altitude LLO requiring $664.9 m/s$ with maneuvers marked in red” – (Whitley et al., 2018)

137 If this transfer option is chosen, the influence of transfer efficiency is very low and therefore marginal to
 138 the ISRU dependencies derived in Chapter 3. In this case transfer dependencies can be neglected and the
 139 location selection can be simplified to only ISRU efficiency.

140 Often however a 100 day transfer time is simply too long for certain applications, as it for example induces
 141 general system lag time and therefore poor dynamics in propellant delivery adjustments in the case of our
 142 mission. For this reason, a second transfer option is analysed which is a direct transfer trajectory between
 143 the NRHO and the surface which features the shortest transfer time of only hours but at the cost of higher
 144 Δv and location dependency. The direct transfer is the subject of the following analysis from here onwards.

145 4.4.3 Data processing

146 In a previous work by Trofimov et al. (2020), a set of possible direct decent trajectories and their
 147 associated landing point and Δv demand were identified. The resulting map of scatter points for the
 148 southern 9:2 NRHO was taken as starting point for the deriving of a global Δv map. Since always the
 149 cheapest option for one location would be chosen, a minimum estimation was performed. This estimation
 150 was done by splitting the map into 20 deg square tiles where constancy is assumed and the lowest value is
 151 set for the whole tile. In preparation for this, the data has been cut from particular high costs trajectories

152 of $\Delta v > 2985.65 \frac{m}{s}$ due to rather leaving non defined tiles at the poles than carrying up to $3.3 \frac{km}{s}$ transfer
153 options over into the final map. This process is visualized in Figure 7 below.

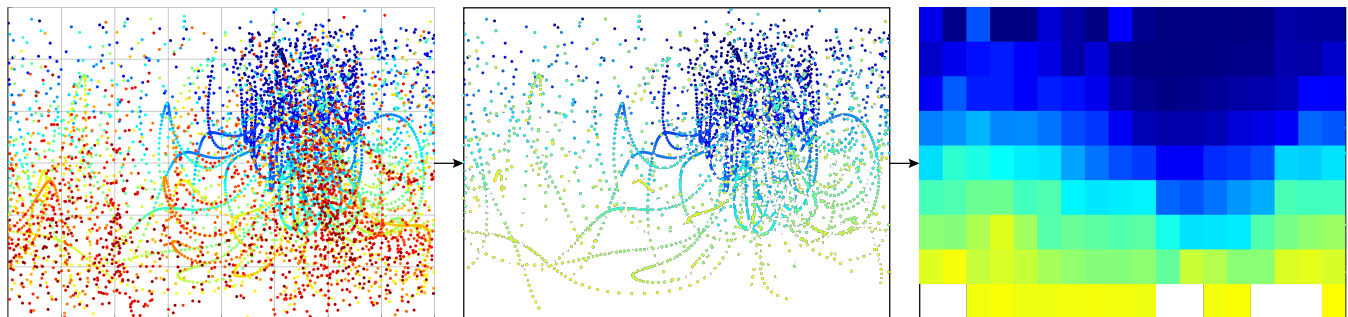


Figure 7. Processing of results from Trofimov et al. (2020) (left) to cutting of data (center) into minimum of 20 deg square tiles (right)

154 The non defined tiles have been interpolated line-wise, which was only necessary in polar regions where
155 there is already a higher geodetic resolution due to equirectangular projection. This leads to our final Δv
156 map, depicted in Figure 8.

157 4.4.4 Result

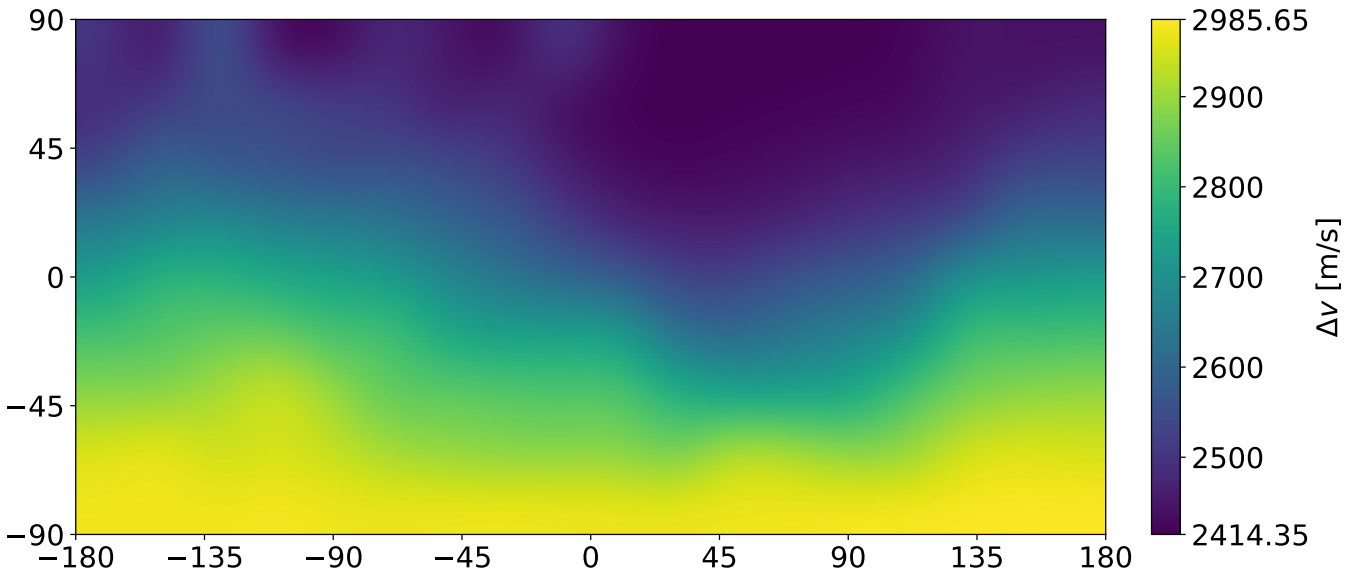


Figure 8. Required Δv for direct decent from Southern 9:2 NRHO to Lunar Surface (bicubic interpolated)

158 Even though this data was computed for the decent only, it will serve as estimation for the ascent as well,
 159 which is holding a bias as those problems are not entirely symmetric. Additionally should be mentioned
 160 that even though a $2414 \frac{m}{s}$ transfer is very viable, a transfer of around $2900 \frac{m}{s}$ might be rather replaced in
 161 a real world scenario by a different transfer strategy, as via LLO with waiting time to save Δv . However, in
 162 this analysis Figure 8 defines $\Delta v(\phi, \lambda)$ globally with $\Delta v_{min} = 2414.35 \frac{m}{s}$ and $\Delta v_{max} = 2985.65 \frac{m}{s}$.

163 4.5 Transport Carrier

164 4.5.1 Reference Launcher

165 To derive associated transport mass costs, the previously determined Δv has to be applied on a specific
 166 launcher. The Argonaut, formerly known as the European Large Logistics Lander (EL3), is chosen as
 167 a starting point for this scenario. The initial configuration is based on the time of writing published
 168 information from the European Space Agency (2023) of 10 000 kg wet mass, 1600 kg drymass and 2100
 169 kg payload. Additionally a Hydrogen, Oxygen propulsion system with an oxidizer fuel ratio of 6 and
 170 400 s of specific impulse are assumed. When this original configuration is applied on our mission with
 171 Δv_{max} (Table 1), the fuel is running out before the round-trip can be completed. Therefore the launcher
 172 configuration has to be altered for our scenario needs.

	Δv [m/s]	$\Delta H2$ [kg]	$\Delta O2$ [kg]	mass [kg]	H2 [kg]	O2 [kg]	payload [kg]
Lunar Surface Maneuvers	2986	-761	+5538.5	10000	762	5538	+2100
Gateway exchange Maneuvers	2986	+1036	-4567	4671	0	971	-2100
ABORT	2986	-275	-1648	3607	1036	971	
				3785	762	-677	
						EMPTY	

Table 1. Mission table with original configuration applied on Δv_{max} showing round-trip insufficiency

173 4.5.2 Launcher Upscaling

174 From there on an up-scaling is performed, where the drymass is kept constant at 1600 kg but fuel is added
 175 until the mission can be completed. The minimal viable system features an empty H₂ tank at arrival at the
 176 Gateway and an empty O₂ tank at the lunar surface. The Iteration scheme of the upscaling is visualized in
 177 Figure 9 which can now converge a minimal viable launcher for any given payload.

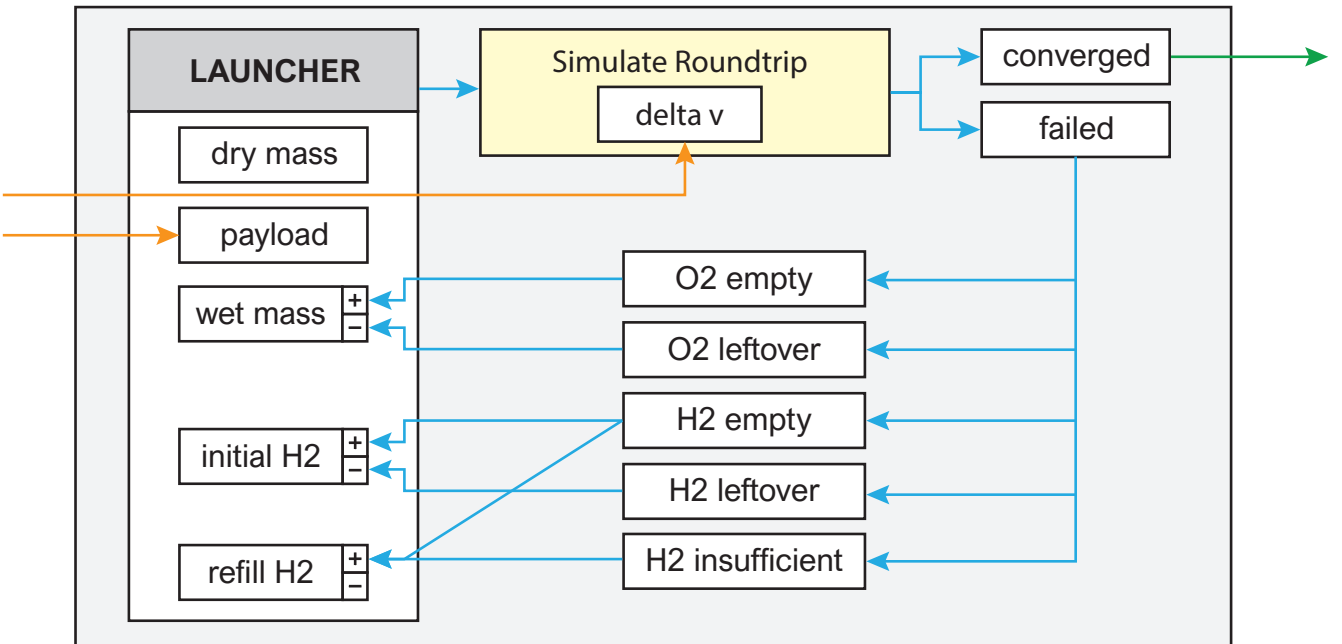


Figure 9. Launcher iteration to converge a roundtrip for a given payload and Δv

178 Since this method of up-scaling is effectively increasing the mass ratio ($r_m = \frac{m_{\text{wet}}}{m_{\text{dry}}}$) of the launcher, this
 179 assumption becomes increasingly unrealistic. Additionally, from the perspective of the fuel depot, Oxygen
 180 is delivered but also Hydrogen is taken away, therefore effectively trading those masses by the exchange
 181 ratio ($r_{ex} = \frac{m_{\text{payload}}}{m_{\text{H2, refill}}}$). In order to bring a decision to what range of launchers shall be analysed, Figure 10
 182 visualises the parameter space between the exchange ratio r_{ex} and the mass ratio of the launcher r_m .

183 Hereby there are 2 sections grayed out, once $r_{ex} < 1$ out of economic reasonableness and second $r_m > 10$
 184 as a soft border of mass ratios for realistic single stage launchers. In order to obtain comparable results, the
 185 mass ratio r_m has to be constant over one set as it represents the efficiency of the launcher. Therefore the
 186 economical reasonable exchange ratios of 1.5 and 2.0 are projected onto the mass ratio and projected back
 187 from its maximum value as a constant, resulting in the 2 chosen frames of:

$$r_m = 8.555 \quad \text{with } 1.5 \leq r_{ex} \leq 3.303$$

$$r_m = 10.688 \quad \text{with } 2.0 \leq r_{ex} \leq 3.889$$

188 To analyse the problem on 2 frames of different mass ratios is proving insight on the sensitivity towards
 189 more efficient launchers in general and their influence on the location selection.

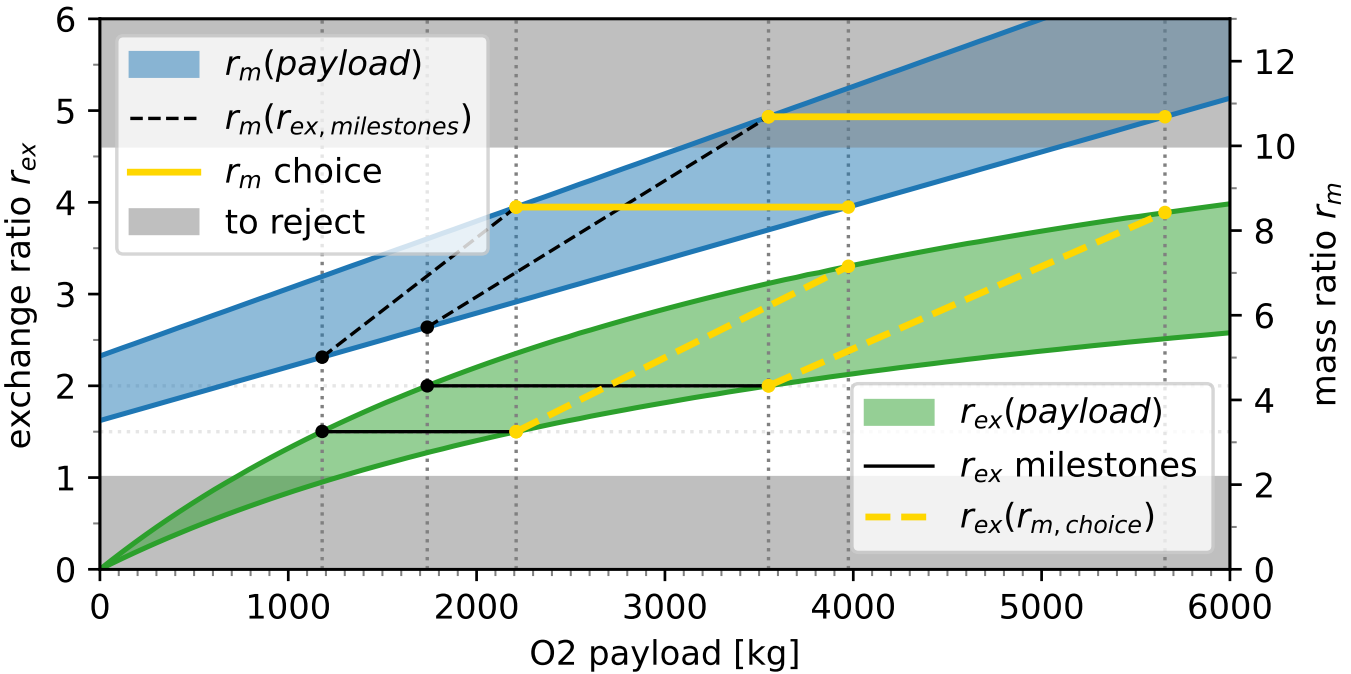


Figure 10. Exchange ratio r_{ex} and mass ratio r_m depending on payload size of the launcher over Δv range

190 4.5.3 Spent Fuel

191 Through another iteration scheme, which is targeting the chosen mass ratio, a launcher can be converged
 192 for a specific Δv . The expended fuel is directly drawn from the simulated round-trip and normalized by the
 193 payload size, which therefore can be combined into a direct mapping from required Δv to the spent fuel
 194 k_{Flight} in kg per kg payload. This dependency can be seen in Figure 11 below for both chosen mass ratios
 195 $r_m = 8.6$ and $r_m = 10.7$. In this comparison, the higher mass ratio $r_m = 10.7$ features a smaller absolute
 196 and relative growth, which concludes that differences in fuel costs decrease in general by an increasing
 197 launcher efficiency.

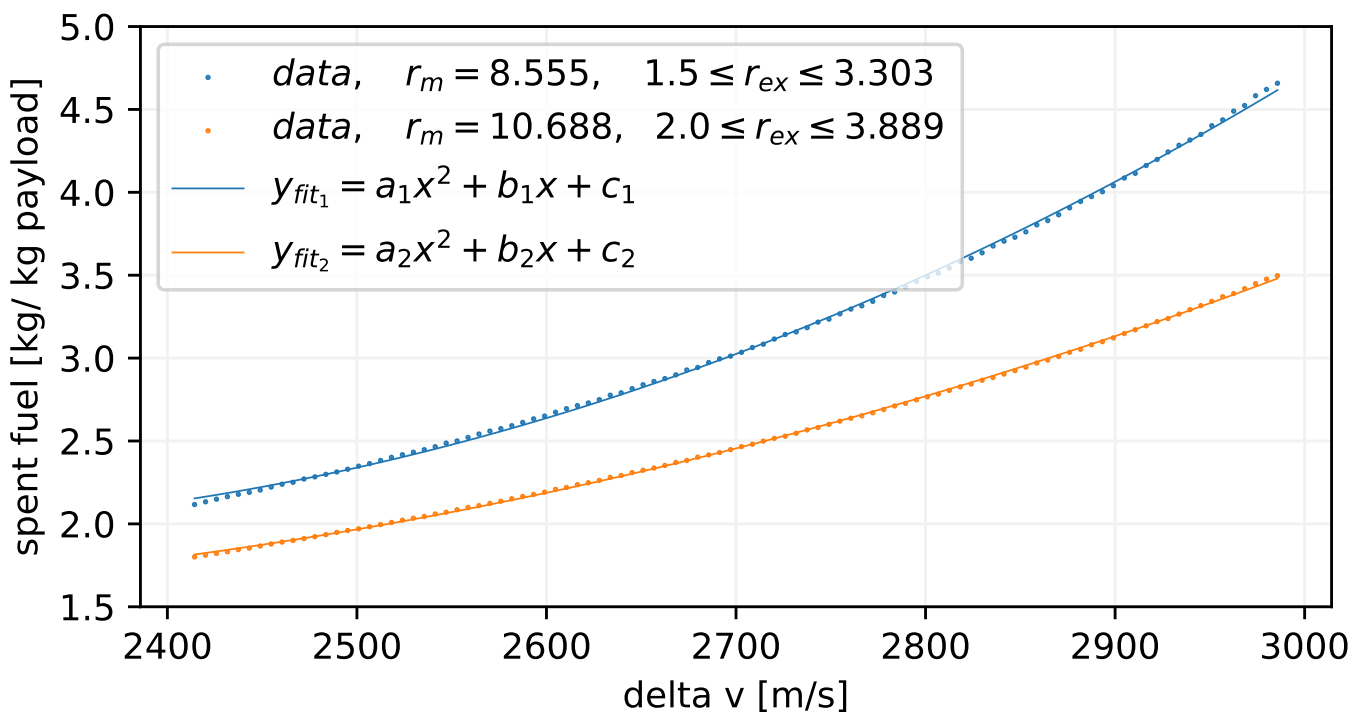


Figure 11. Relationship between required Δv and spent fuel k_{Flight} for both mass ratios

5 JOINED MODEL

199 5.1 Total Cost Modelling

200 When both influences from Section 3 and Section 4 are combined, the comparable mass costs have to be
 201 drawn from the mission scenario. Rather than assuming all expended fuel as transport cost, a separation of
 202 the fuel components is done, due to the reason that the Oxygen is not being shipped from Earth but rather
 203 fully supplied by the ISRU facility.

204 5.1.1 Fix Costs

205 In order to meet the additional demand of Oxygen per year, that the launcher requires for transport,
 206 the ISRU facility is scaled up linearly by its ISRU costs per kg Oxygen k_{ISRU} for each location and its
 207 corresponding fuel requirements. The scaling factor originates from the base configuration costs from
 208 Figure 4 and its annual production, which gives: $k_{\text{ISRU}}(\phi, \lambda) = \frac{K_{\text{base}}(\phi, \lambda)}{23.9t}$. The additional Oxygen demand
 209 per year is derived by the oxidiser-fuel-ratio r_{of} and the spent fuel k_{Flight} depending on the 2 selected
 210 mass ratios $r_m \in \{8.6, 10.7\}$. Therefore the fix costs, which represent the Earth supplied mass for the
 211 construction of the ISRU facility are:

$$K_{\text{Fix}}(\phi, \lambda, r_m) = K_{\text{base}}(\phi, \lambda) + k_{\text{ISRU}}(\phi, \lambda) \cdot k_{\text{Flight}}(\phi, \lambda, r_m) \cdot \frac{r_{\text{of}}}{r_{\text{of}} + 1} \quad (4)$$

212 5.1.2 Dynamic Costs

213 The expended Hydrogen is considered fully as mass cost since it is taken from the Lunar Gateway depot
 214 and assumed to be delivered by Earth. Hereby the cost level of the Lunar Gateway and the lunar surface
 215 are simplified as equal from Earth to be comparable, which rather overestimates the Hydrogen's cost in
 216 comparison to costs on the lunar surface when supplied from Earth. Therefore the dynamic costs, which
 217 represent the Earth supplied mass for Hydrogen on the Lunar Gateway per year t are:

$$K_{\text{Dynamic}}(\phi, \lambda, t, r_m) = t \cdot k_{\text{Flight}}(\phi, \lambda, r_m) \cdot \frac{1}{r_{\text{of}} + 1} \quad (5)$$

218 5.1.3 Total Costs

219 Combining both K_{Fix} and K_{Dynamic} , the final total costs of the mission over location and time are:

$$K_{\text{Total}}(\phi, \lambda, t, r_m) = K_{\text{Fix}}(\phi, \lambda, r_m) + K_{\text{Dynamic}}(\phi, \lambda, t, r_m) \quad (6)$$

220 5.2 Total Cost Result

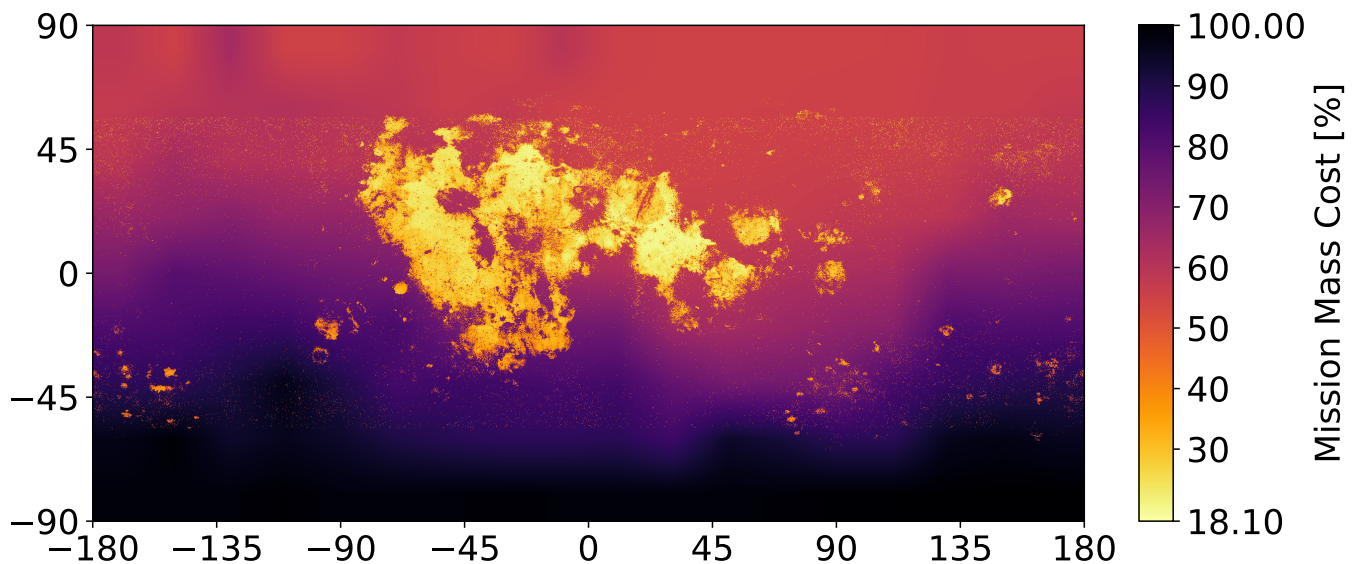


Figure 12. Location dependent total mission cost K_{Total} in % with $t = 20$ years and $r_m = 8.6$

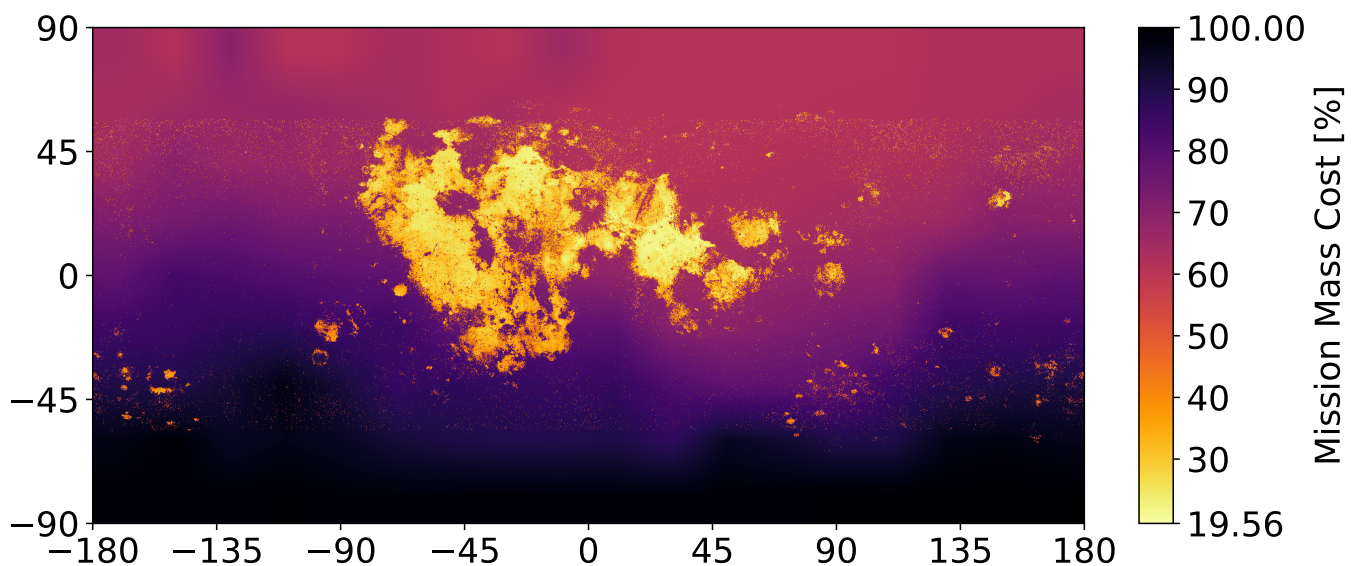


Figure 13. Location dependent total mission cost K_{Total} in % with $t = 20$ years and $r_m = 10.7$

6 RESULTS

6.1 Flight Cost Influences

Through the availability of the long duration transfer strategy (Section 4.4.2) which is able to diminish location dependencies, as well as insignificant planetary influences (Section 4.4.1), the effects on the missions location selection are eliminated by an assumable uniform Δv requirement.

Only under the short duration transfer strategy, location dependent Δv requirements are prominent (Section 4.4.4) which translate to a significant difference in spent fuel (Section 4.5.3). On the other side at the ISRU influence, Ilmenite reduction introduces vast location dependencies (Section 3.2.2), which overshadow the differences in the spent fuel, resulting in an ISRU feature dominated total cost when both influences are combined (Section 5.2).

6.2 Flight Cost Negligibility

The specific influence on location selection and its most optimal choice between flight costs are neglected or not, top 10 locations of

	#1	#2	#3	#4	#5	#6	#7	#8	#9	#10
ISRU	$T_{15,40}$	$T_{14,24}$	$T_{16,41}$	$T_{14,23}$	$T_{16,40}$	$T_{12,23}$	$T_{13,24}$	$T_{17,40}$	$T_{10,31}$	$T_{16,42}$
J. t = 0	$T_{15,40}$	$T_{16,41}$	$T_{16,40}$	$T_{14,24}$	$T_{10,31}$	$T_{14,23}$	$T_{15,41}$	$T_{15,43}$	$T_{16,42}$	$T_{17,40}$
J. t = 10	$T_{15,40}$	$T_{16,41}$	$T_{16,40}$	$T_{10,31}$	$T_{15,43}$	$T_{15,41}$	$T_{15,42}$	$T_{16,42}$	$T_{17,40}$	$T_{14,24}$
J. t = 20	$T_{15,40}$	$T_{16,41}$	$T_{16,40}$	$T_{15,43}$	$T_{15,41}$	$T_{15,42}$	$T_{10,31}$	$T_{16,42}$	$T_{14,41}$	$T_{17,40}$
	#1	#2	#3	#4	#5	#6	#7	#8	#9	#10
ISRU	$T_{79,204}$	$T_{80,201}$	$T_{81,201}$	$T_{72,118}$	$T_{80,200}$	$T_{80,204}$	$T_{81,199}$	$T_{72,116}$	$T_{78,176}$	$T_{73,120}$
J. t = 0	$T_{79,204}$	$T_{80,201}$	$T_{81,201}$	$T_{80,200}$	$T_{80,204}$	$T_{81,199}$	$T_{79,203}$	$T_{80,203}$	$T_{81,200}$	$T_{78,176}$
J. t = 10	$T_{79,204}$	$T_{80,201}$	$T_{80,204}$	$T_{81,201}$	$T_{80,200}$	$T_{79,203}$	$T_{76,206}$	$T_{80,203}$	$T_{81,199}$	$T_{76,202}$
J. t = 20	$T_{79,204}$	$T_{80,204}$	$T_{80,201}$	$T_{76,206}$	$T_{77,212}$	$T_{79,203}$	$T_{78,218}$	$T_{80,200}$	$T_{76,202}$	$T_{75,206}$

Table 2. Top 10 best mission locations compared between ISRU model and Joined model (J.) after t years in pixel area relation resized square tiles ($T_{\phi \text{ index}, \lambda \text{ index}}$) with $5^\circ \phi, \lambda$ tiles (top) and $1^\circ \phi, \lambda$ tiles (bottom). Indices starting at zero on $(90^\circ \phi, 0^\circ \lambda)$ with 0° to 360° Longitude range. Data from mass ratio $r_m = 8.6$.

7 DISCUSSION

CONFLICT OF INTEREST STATEMENT

233 The authors declare that the research was conducted in the absence of any commercial or financial
234 relationships that could be construed as a potential conflict of interest.

AUTHOR CONTRIBUTIONS

235 The Author Contributions section is mandatory for all articles, including articles by sole authors. If an
236 appropriate statement is not provided on submission, a standard one will be inserted during the production
237 process. The Author Contributions statement must describe the contributions of individual authors referred
238 to by their initials and, in doing so, all authors agree to be accountable for the content of the work. Please
239 see here for full authorship criteria.

FUNDING

240 This research was conducted without any institutional funding. Publication fees are covered by the Technical
241 University of Munich's support for open access publishing.

ACKNOWLEDGMENTS

242 This is a short text to acknowledge the contributions of specific colleagues, institutions, or agencies that
243 aided the efforts of the authors.

DATA AVAILABILITY STATEMENT

244 This work is providing open source on all processing steps performed in the corresponding Python
245 Notebooks along with all resources in full resolution in the papers Git-Repository [Link](#).

REFERENCES

- 246 [Dataset] David E. Smith (2015). 2009 lunar orbiter laser altimeter radiometry data set, lro-l-lola-3-radr-
247 v1.0. doi:10.17189/1520639
- 248 [Dataset] Ernie Wright and Noah Petro (2019). SVS: CGI Moon Kit — svs.gsfc.nasa.gov. <https://svs.gsfc.nasa.gov/4720>. [Accessed 29-07-2023]
- 249 [Dataset] European Space Agency (2023). Argonaut - technical details. https://www.esa.int/Science_Exploration/Human_and_Robotic_Exploration/Exploration/Argonaut. [Accessed 08-09-2023]
- 250 Guerrero-Gonzalez, F. J. and Zabel, P. (2023). System analysis of an ISRU production plant: Extraction of
251 metals and oxygen from lunar regolith. *Acta Astronautica* 203, 187–201. doi:10.1016/j.actaastro.2022.
252 11.050
- 253 Lee, D. E. (2019). National aeronautics and space administration (nasa) white paper: Gateway destination
254 orbit model: A continuous 15 year nrho reference trajectory
- 255 Nelson, D. M., Koeber, S. D., Daud, K., Robinson, M. S., Watters, T. R., Banks, M. E., et al. (2014).
256 Mapping lunar maria extents and lobate scarps using lroc image products. *Lunar Planet. Sci.* 45, 2861

- 260 Perrin, T. M. and Casler, J. G. (2016). Architecture study for a fuel depot supplied from lunar resources. In
261 *AIAA SPACE 2016* (American Institute of Aeronautics and Astronautics). doi:10.2514/6.2016-5306
- 262 Sato, H., Robinson, M. S., Lawrence, S. J., Denevi, B. W., Hapke, B., Jolliff, B. L., et al. (2017). Lunar
263 mare tio 2 abundances estimated from uv/vis reflectance. *Icarus* 296, 216–238. doi:10.1016/j.icarus.
264 2017.06.013
- 265 Trofimov, S., Shirobokov, M., Tselousova, A., and Ovchinnikov, M. (2020). Transfers from near-
266 rectilinear halo orbits to low-perilune orbits and the moon’s surface. *Acta Astronautica* 167, 260–271.
267 doi:10.1016/j.actaastro.2019.10.049
- 268 Whitley, R., Davis, D., Burke, L., McCarthy, B., Power, R., McGuire, M., et al. (2018). Earth-moon near
269 rectilinear halo and butterfly orbits for lunar surface exploration